applied sciences

MDPI

Article

Intermolecular Interactions in Mixed Choline Acetate and Maleic Acid Systems

Simone Di Muzio [1,2], Annalisa Paolone [1], Francesco Trequattrini [1,3] and Oriele Palumbo [1,*]

[1] Istituto dei Sistemi Complessi, Consiglio Nazionale delle Ricerche, P.le Aldo Moro 5, 00185 Rome, Italy; simone.dimuzio@ifn.cnr.it (S.D.M.); annalisa.paolone@roma1.infn.it (A.P.); francesco.trequattrini@uniroma1.it (F.T.)
[2] Istituto di Fotonica e Nanotecnologie, Consiglio Nazionale delle Ricerche, Piazza Leonardo da Vinci, 32, 20133 Milano, Italy
[3] Department of Physics, Sapienza University of Rome, P.le Aldo Moro 5, 00185 Rome, Italy
* Correspondence: oriele.palumbo@roma1.infn.it

Abstract: Mixed systems based on ionic liquids are promising innovative solvents due to their properties, which are strictly connected to the interactions that arise among the components. The present work investigates the intermolecular interactions of a mixed choline acetate and maleic acid system and their modifications with increasing acid content. MM/DFT calculations provided indications about the possible geometric configurations of the systems while Non-Covalent Interaction analysis was useful to describe and distinguish secondary interactions. The number of available configurations decreases at high acid concentration. Moreover, intramolecular hydrogen bonding was observed in all configurations except that in the most stable one of the lowest acid content mixture. Concomitantly, far-infrared spectroscopy was used to investigate intermolecular interactions and provided support to the computational results.

Keywords: hydrogen bonding; choline acetate; maleic acid; MM/DFT calculation; infrared spectroscopy

Citation: Di Muzio, S.; Paolone, A.; Trequattrini, F.; Palumbo, O. Intermolecular Interactions in Mixed Choline Acetate and Maleic Acid Systems. *Appl. Sci.* **2024**, *14*, 11402. https://doi.org/10.3390/app142311402

Received: 4 November 2024
Revised: 3 December 2024
Accepted: 6 December 2024
Published: 7 December 2024

1. Introduction

In recent years, the development of alternative and innovative solvents has gained significant attention to achieve more sustainable chemical processes; these solvents include ionic liquids (ILs) and deep eutectic solvents (DESs) [1–4]. Despite their structural and compositional differences, both classes of solvents exhibit a range of unique and desirable physicochemical properties. These include intrinsic low vapor pressures, reduced environmental volatility, high thermal and chemical stability, as well as tunable polarity and solvating abilities [5–11]. Moreover, ILs and DESs are recognized for their low toxicity [12] compared to conventional organic solvents, and their biodegradability enhances their environmental compatibility, making them attractive for applications in green chemistry [13,14]. Their ability to dissolve a broad spectrum of materials [15–18] is further complemented by a wide liquidus range, enabling their use at different temperatures while avoiding the risk of crystallization or phase separation [19]. The ongoing research on the customizability of ILs and DESs has further highlighted their potential, as their physicochemical properties can be fine-tuned by varying the cation/anion pair in ILs or the hydrogen bond donor/acceptor composition in DESs. This allows for the precise optimization of solvent characteristics for specific applications, such as enhancing solubility, improving reaction rates, or facilitating separation processes [20]. It becomes clear that the unique and distinctive chemical–physical properties of these systems are profoundly influenced by the intricate intermolecular interactions that arise between the components. Therefore, a precise and in-depth chemical–physical characterization of these interactions is crucial for gaining a comprehensive understanding of the macroscopic behavior of these liquids, enabling us to fine-tune their properties for targeted applications.

In this work, we propose mixtures based on choline acetate (ChAc), classifiable as an ionic liquid, combined with the hydrogen bond donor (HBD) maleic acid (MA) (Figure 1), with the aim of developing low-melting binary mixtures. The capability of maleic acid to act as H-bond donor in the formulation of deep eutectic solvents can be explained considering the by-carboxylic nature of this acid, which facilitates strong H-bonding interactions [21]. Choline is a widely utilized cation in the formulation of ionic liquids and deep eutectic solvents, with a variety of anions being paired with it. Among these, choline chloride (ChCl) is by far the most extensively studied combination. In contrast, systems based on ChAc have received comparatively less attention. Exploring the physicochemical properties of ChAc—where the acetate anion acts as a weak organic base—in combination with organic acids such as maleic acid could provide valuable insights into their interactions and expand the potential applications of these systems. Following our previous research [22], we propose three different molar ratios: a choline acetate-rich mixture (ChAc-MA 2-1), an equimolar mixture (ChAc-MA 1-1), and a maleic acid-rich mixture (ChAc-MA 1-2). Indeed, a study of the system based on HBD concentration is crucial for a deeper investigation of the secondary interactions. Varying the amount of acid, for instance, can directly impact the number of hydrogen bonds within the mixtures, offering valuable insights into how these interactions shape the overall behavior. As observed by our previous work [22], the increasing amount of acid leads to greater cross-linking through hydrogen bond interactions, as evidenced by mid-IR spectroscopy results reporting variable shifts in the OH and C=O stretching bands as a function of acid concentration, and by radial distribution functions obtained from the analysis of classical molecular dynamics trajectories. The phenomenon of cross-linking through hydrogen bonding in deep eutectic solventsrepresents a fascinating avenue of study. For instance, Ferreira et al. demonstrated how the hydrogen bonding interactions between choline chloride and organic alcohols [23] contribute to the formation of a robust network, directly influencing the viscosity of the system and thermal stability. These findings underline the importance of examining hydrogen bonding networks, particularly in the context of novel DES systems such as those based on maleic acid, which may exhibit comparable cross-linking characteristics.

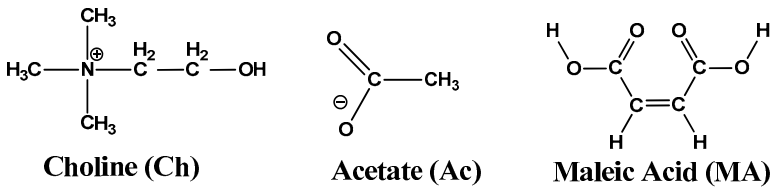

Figure 1. Structures and abbreviations of the ions involved in the studied mixtures.

To explore the intermolecular interactions, in the present paper, we extend the previous measurements by performing a wide temperature range infrared spectroscopy study in the far-IR region, a spectral range known to reveal bands related to hydrogen bonding and van der Waals dispersion forces [24–37]. Indeed, conducting studies as a function of temperature is particularly intriguing, as it reveals how spectral bands change in response to molecular reorganization during phase transitions. As temperature changes, the spatial arrangement of molecules undergoes significant transformations, especially during the solid–liquid transition. In the solid state, hydrogen bonding is highly directional and organized, making it easier to detect and analyze these interactions. By examining the temperature-dependent changes, we can gain valuable insights into the dynamics of intermolecular forces, particularly hydrogen bonding, and how they shape the macroscopic properties of the system. This understanding is crucial for tailoring materials with desired characteristics and behaviors. Moreover, the spectral variations observed by varying the temperature can be attributed not only to phase transitions but also to the thermal evolution of the different geometric conformations, which is governed by the Boltzmann distribution, with higher temperatures allowing for larger energy states to be accessible. It

is important to note that in the liquid phase, conformers evolve with temperature, allowing for a continuous transition between different molecular arrangements. However, when systems undergo vitrification or solidification, the mobility of the molecules is significantly reduced, resulting in them becoming trapped in a particular configuration.

In order to better interpret the complex region of the far-infrared (FIR), a careful computational investigation at the density functional theory (DFT) level is necessary. To this end, we deepened the computational investigation previously reported [22] by calculating all the possible geometric configurations and computing the infrared spectra only for those with significant weight in the Boltzmann distribution. The Non-Covalent Interaction (NCI) analysis performed on the lowest energy structures of each composition was proved to be particularly useful to describe and distinguish secondary interactions, such as hydrogen bonding and van der Waals forces [38–41].

2. Materials and Methods

Choline acetate and maleic acid were purchased from Merck with purities higher than 95% and 99%, respectively. Each compound was dried in vacuum for 8 h at 330 K before samples preparation. Three mixtures at different molar ratios were prepared by mixing the dried starting materials, following an already established procedure [22]. The mixtures, labeled as ChAc-MA 2-1, ChAc-MA 1-1 and ChAc-MA 1-2,were formulated by mixing the components in the molar ratio described by the label, i.e., the ChAc-MA 2-1 mixture was obtained mixing proper amounts of ChAc and MA in molar ratio acetate–acid equal to 2:1. The mixtures were heated at 350 K under stirring until a fully liquid phase appeared. Afterward, the samples were heated at 330 K for 8 h, dried in vacuo, and stored in an argon atmosphere in sealed glass vials to avoid any external contaminations. All the obtained samples were viscous liquids at room temperature. ChAc-MA mixtures 2-1, 1-1 and 1-2 displays only glass transitions around 194 K, 199 and 241 K (see Figure S1), respectively.

Infrared spectra were recorded in the far-IR range at the AILES beamline of Synchrotron Soleil in Paris by means of a Bruker IFS125 HR spectrometer, equipped with a 6 μm Si-coated beamsplitter and a bolometer as a detector. The temperature was varied by means of a Cryomec cryopump. A drop of liquid was placed between two diamond optical windows separated by a spacer of 10 μm inside a sealed optical cell. The experimental results were compared with DFT calculations. Preliminary conformational analysis was conducted at a classical molecular mechanic level: all the obtained configurations were afterwards optimized at the B3LYP/6-31G** level of theory applying an implicit solvation model (PCM). Many studies [42,43] have suggested that the proper value of the dielectric constant for these systems is approximatively between 10 and 20; therefore, for the present calculations, the value of the dielectric constant was fixed at $\varepsilon = 15$, according to the polarity observed in analogs systems [42,43]. The MM/DFT calculations provided a large number of possible configurations; nevertheless, configurations actually describing the geometric arrangement of molecules in the liquid phase are restricted and significantly influenced by their relative energies and their weight in the Boltzmann distribution. This led us to select, among all the obtained configurations, those falling within an energy range of 6 kJ/mol compared to the most stable ones [44]. Frequency calculations were carried out only for these subsets. All calculations were performed by means of the Spartan20 [45]. The Non-Covalent Interaction analysis was performed by means of the Multiwfn package [46] and the results were visualized with the VMD software [47].

3. Results

3.1. Computational Results

A careful DFT computational analysis was conducted by varying the number of composing molecules according to the experimental concentration. In agreement with the labeling used for the mixed samples, the corresponding simulated clusters were labeled as reported in Table 1.

Table 1. Labelling and composition of the proposed systems.

	Number of ChAcMolecules	Number of MA Molecules
ChAc-MA 2-1	2	1
ChAc-MA 1-1	1	1
ChAc-MA 1-2	1	2

Previous work [22] showed that in the present systems, the coordination of cations and anions in the liquid phase is influenced by strong H-bond interactions between the hydroxyl groups of choline (OH) and the carboxylate oxygens of acetate (O=C-O$^-$); in addition, in all the models of liquid bulks, maleic acids act as hydrogen bond donors (HBDs) [22], being able to donate strong H-bonds to acetate and other acid molecules. For these reasons, we decided to set the input for MM/DFT calculations, paying particular attention to the orientation of the H-bond donors and acceptors groups with the aim of focusing on these interactions. The optimized lowest energy configurations obtained for each composition are reported in Figure 2. Within a range of 6kJ/mol, with respect to the most stable one, we obtained three possible configurations for the 2-1 mixture (see Figure 2a–c), two configurations for the 1-1 composition (Figure 2d,e) and only one (Figure 2f) for the 1-2 structure.

The energy separations between the configurations are reported in Table 2, while the main distances and angles obtained for these configurations are reported in the supporting info; see Table S1. The calculated absolute energies of the six configurations are also reported in Table S2.

The 2-1 composition is formulated by an excess of choline acetate. Being a dicarboxylic organic acid, MA serves as a bidentate hydrogen bond donor, allowing for coordination with equal probability at either of its carboxylic groups. In fact, in the most stable configuration (Figure 2a) MA is engaged in a double H-bond, simultaneously coordinating one of the two choline cations (H18---O8, see Figure 2a) and the acetate of the other ion pair (H16---O2). Indeed, the calculated H18---O8 and H16---O2 bond lengths are 1.57 and 1.43 Å, respectively, with the corresponding angles close to 180°, and are compatible with the characteristic distances of a strong hydrogen bond [48]. Configuration b (Figure 2b), although separated from the previous one by a small barrier (0.8 kJ/mol), shows an important difference in the coordination: MA is arranged with an intramolecular H-bond between H18 and O4, which induces a closed configuration of the maleic acid due to a rotation of one of the carboxylic acid groups. The other carboxylic group is still engaged in the hydrogen bond donation to one of the two acetates. The increased stability observed in the first configuration may arise from the open structure of the acid, facilitating the more efficient cross-linking and structural stabilization of the whole system. Configuration c (Figure 2c) is the less stable with a considerable energy difference of more than 5 kJ/mol, with respect to the lowest energy value. In this case, the maleic acidis again arranged in a closed configuration with an intramolecular H-bond and an intermolecular H-bond with one of the acetates. However, the comparison of the bond distances (Table S1 of the Supporting Information) suggests that the intramolecular H-bond becomes slightly stronger in configuration b than in the c one (since the H18-O4 distances is larger in configuration c), while concomitantly the choline cation is closer to the acetate anion not involved in the intermolecular H-bond. The intermolecular H-bond, instead, becomes stronger in configuration b (since the H16-O5 distances is larger in b). Indeed, the formation of strong intermolecular bonds contributes to the stability of the whole system, as observed for the most stable configuration a, where the main occurring interactions are of this type. Moreover, in all configurations (a, b and c), all the acetates are engaged in at least one H-bond with either choline or maleic acid.

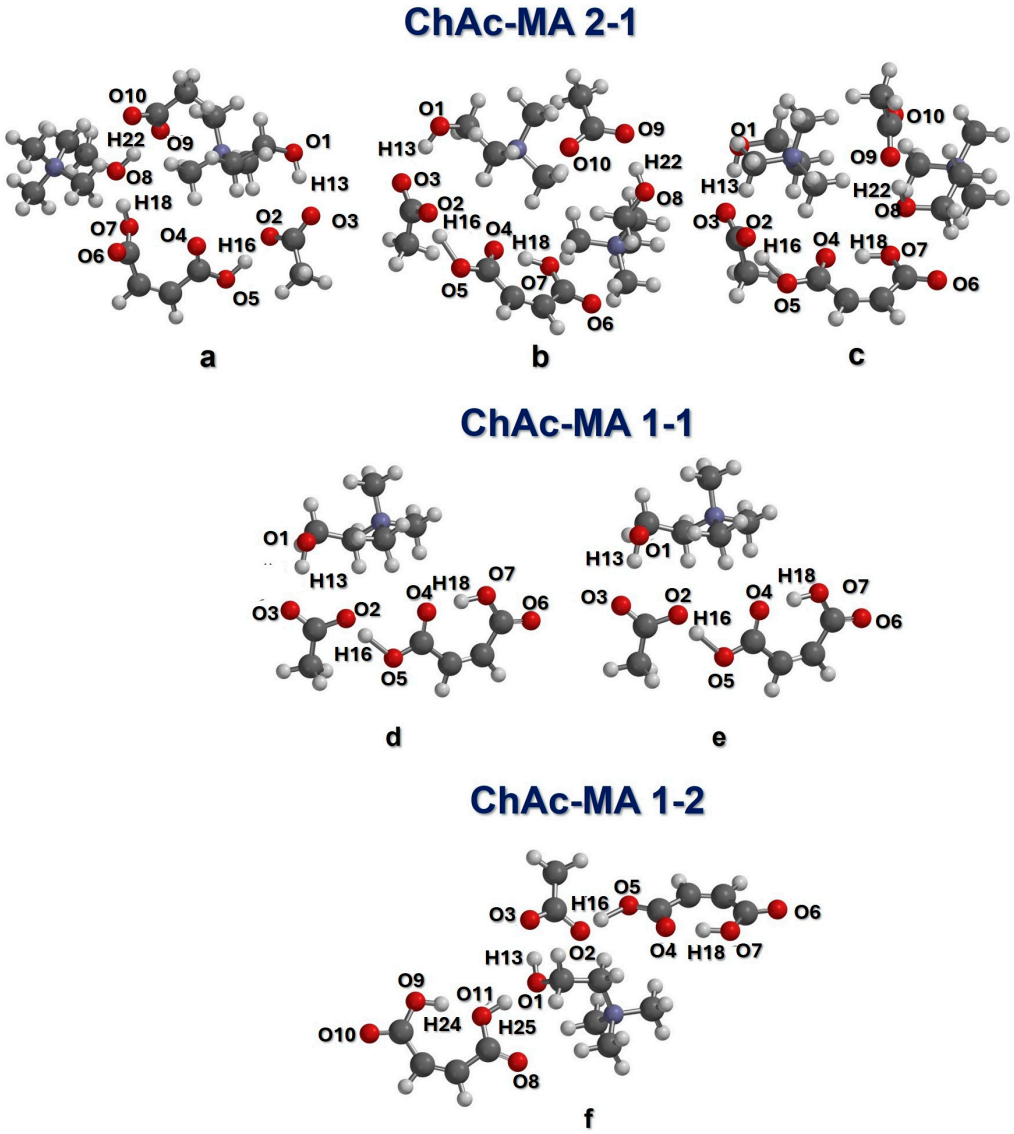

Figure 2. MM-B3LYP/6-31G** optimized geometries for the three compositions: ChAc-MA 2-1 (**a**–**c**), ChAc-MA 1-1 (**d**,**e**) andChAc-MA 1-2 (**f**).

Table 2. Energy separation between the configurations obtained for ChAc-MA 2-1 and ChAc-MA 1-1 at B3LYP/6-31G** level of theory.

ChAc-MA 2-1	ΔE(kJ/mol)	ChAc-MA 1-1	ΔE(kJ/mol)
Configuration a	0.00	Configuration d	0.00
Configuration b	0.82	Configuration e	0.19
Configuration c	5.75		

For the 1-1 concentration, our MM/DFT calculations identified only two configurations that met our energy criteria, separated by only 0.19 kJ/mol. In both equimolar configurations d and e (panel d and e of Figure 2, respectively) all components are bounded via strong H-bonds: the acetate is coordinated by MA through the carboxyl proton H16 and by the choline trough the hydroxyl proton H13, forming a bridged structure composed by a double H-bond, H16 (MA)—O2(Ac)—C--O3(Ac)—H13(Ch). Both configurations show MA arranged with an intramolecular hydrogen bond (H18-O4). This can be rationalized by considering the lower number of acceptor groups in the mixture: the dicarboxylic acid, therefore, has fewer HBA groups to coordinate with and arranges itself to maximize the

number of H-bonding, also forming an intramolecular bond. The two configurations of d and e exhibit very slight differences in terms of geometry, as also evidenced by the nearly identical energy level of the two structures. Figure 1 and Table SI-1, in fact, illustrate that the coordination between the two conformers is quite similar. However, there are slight variations in the hydrogen bond angle O1-H13-O3, measuring 170.9° in configuration d and 173.0° in configuration e. Additionally, a difference is observed in the dihedral angles C8-O4-H18-O7, which are 26.8° in the more stable configuration (d) and 33.1° in the less stable configuration (e). These subtle geometric differences suggest that the two structures are nearly equivalent, both in terms of geometry and energy.

The last examined concentration, ChAc-MA 1-2, exhibits an excess of acid: our calculations indicate the presence of a single energetically accessible configuration in which both molecules of MA are arranged with intramolecular H-bond. Similarly to the other compositions previously described, the acetate is coordinated through the OH group of choline and the hydroxyl group of maleic acid. As mentioned above, in all clusters, the intermolecular distances between protons located on the donor group and the oxygen of the acceptor ones are consistent with strong H-bonding, with bond lengths ranging between 1.5 and 1.7 Å and all related angles approaching 180°. These criteria match the parameters provided by the IUPAC, which define an interaction as a strong hydrogen bond [48,49].

In configurations where intramolecular hydrogen bonding occurs in maleic acid, it is noteworthy that the H-bond between the acid and the acetate extends towards the oxygen of the carboxylate group in the anion: indeed, taking configuration b as example, the bond length of O5—H16, which corresponds to the proton–oxygen distance in the carboxyl portion of MA, is 1.51 Å, while the distance H16---O2 (from acid to acetate) is 1.03 Å. These observations lead us to hypothesize the establishment of a proton transfer (PT) mechanism, which was observed in all structures, except for configuration a, where the intramolecular H-bonding in MA is not present. Indeed, this phenomenon occurs even at other concentrations, and the bonds distances are similar and close to those described for the 2-1 composition (See Table S1).

The proton transfer occurs between molecules where the establishment of an acid-base equilibrium is possible. The presence of intramolecular hydrogen bonds in maleic acid, as revealed by almost all computed structures, can promote the proton transfer mechanism. This suggests that the intramolecular H-bond acts as the mechanism that makes proton transfer favorable, providing further confirmation of the significant role of H-bonds in facilitating this process. Furthermore, previous study has experimentally and computationally demonstrated, through vibrational spectroscopy, molecular dynamics simulations and DFT calculations, that in cholinium maleate (ChMal) ionic liquid, the maleate anion tends to arrange itself in a closed structure, establishing a strong intramolecular hydrogen bond [50].

To better describe the mechanism and the thermodynamics related to the PT, we computed the Gibbs energy (ΔG^0_r) for two proton transfer reactions. For simplicity, we started by considering the reaction without the presence of the counterion, namely the choline, as indicated in Equation (1). Considering the significant stabilization effect on the ion pair exerted by choline, we extended the calculation introducing the cation, as reported in Equation (2). Both reactions are attempts to describe the proton transfer mechanism. Therefore, the reactants considered are maleic acid and acetate anion (or choline acetate in the case of Equation (2)). When the proton is transferred from maleic acid to acetate, a mechanism is established that leads to the protonation of the acetate, with the formation of acetic acid and maleate. The ΔG^0_r was computed at the B3LYP/6-31G** level of theory and was obtained as the difference between the products and reactants.

$$\text{Maleic Acid} + [\text{Acetate}]^- \text{ ---> Acetic Acid} + [\text{Maleate}] \quad (1)$$

$$\text{Maleic Acid} + \text{Choline Acetate ----> Acetic Acid} + \text{Choline Maleate} \quad (2)$$

The computed Gibbs free energy of both reactions demonstrates that proton transfer is thermodynamically favored, as $\Delta G^0{}_r(1)$ is -362 kJ/mol and $\Delta G^0{}_r(2)$ is -44 kJ/mol. The notable difference between these two values arises from the strong coordination of acetate to choline in the second reaction, thereby diminishing its reactivity.

The proton transfer occurs between molecules where an acid-base equilibrium can be established. The significant difference in the pKa values [51] of maleic acid (pKa1 $\approx$ 1.9, pKa2 $\approx$ 6.1) and acetic acid (pKa $\approx$ 4.76) plays a critical role in this mechanism. Maleic acid, being a much stronger acid than acetic acid, has a higher tendency to donate protons, driving the proton transfer process. The stronger acidity of maleic acid compared to acetic acid facilitates the formation of the maleate anion, making the proton transfer thermodynamically favorable. This contrast in acidity highlights the role of the relative acid strengths in determining the direction of the proton transfer, where the proton moves from the stronger acid (maleic acid) to the weaker acid (acetate). Additionally, the presence of intramolecular hydrogen bonding in maleic acid further promotes this mechanism, as it stabilizes the structure and lowers the energy barrier for proton transfer.

An alternative and complementary way to describe and visualize intermolecular interactions can be performed by means of the NCI calculations. The role of NCIs can be investigated by studying the Laplacian of electron density, $\nabla^2\rho$, as the sign of its eigenvalue λ_2 represents a good way to discriminate van der Waals, hydrogen bonds and repulsive interactions. The NCI surfaces were computed for the most stable configuration obtained for each composition, as described at the beginning of this paragraph, and reported in Figure 3.

In the isosurfaces, each color corresponds to specific interactions: the red one indicates strong repulsion while green and blue ones describe van der Waals and hydrogen bond interactions, respectively. In all the considered structures, the presence of intense H-bond interactions was observed, as demonstrated by the existence of blue zones between the hydrogens involved in the coordination of acetate. As previously stated, the most stable conformer in the 2-1 composition involves maleic acid in a double coordination, establishing interactions with acetate and choline oxygen through a dual hydrogen bond. This configuration represents the only scenario in which maleic acid assumes an open form, lacking intramolecular hydrogen bonding. We previously stated that the intramolecular H-bond facilitates the proton transfer process between acetate and maleic acid. A confirmation of our hypothesis can be sought in the NCI analysis. Taking as an example the coordination between acid and acetate in Figure 3a, a delocalization of the acidic proton between the carboxyl group of acid and carboxylate of anion was observed. As previously described, the bond distance obtained from DFT models (see Table SI-1) suggested that the proton is more strongly bound to acid: this clearly indicates that the proton transfer does not occur. The NCI isosurfaces confirmed this claim, displaying a toroidal-shaped repulsive region (highlighted in red) between the acid-bound proton and the oxygen of the carboxylate of acetate. Conversely, in the 1-1 and 1-2 mixtures, a contrasting scenario was observed, in which maleic acid is arranged in closed configuration as a result of the intramolecular H-bond. The resulting proton transfer can be confirmed since the electrostatic repulsion zone between the bridging H-bond of acid and acetate is located between the formed acetic acid and the maleate anion.

In addition to the hydrogen bonds, which contribute significantly to the stabilization effect in these mixtures, our calculations unveiled pronounced green-colored regions, attributed to the presence of van der Waals interactions. This phenomenon was observed in all compositions but exhibited heightened intensity in the 2-1 mixture.

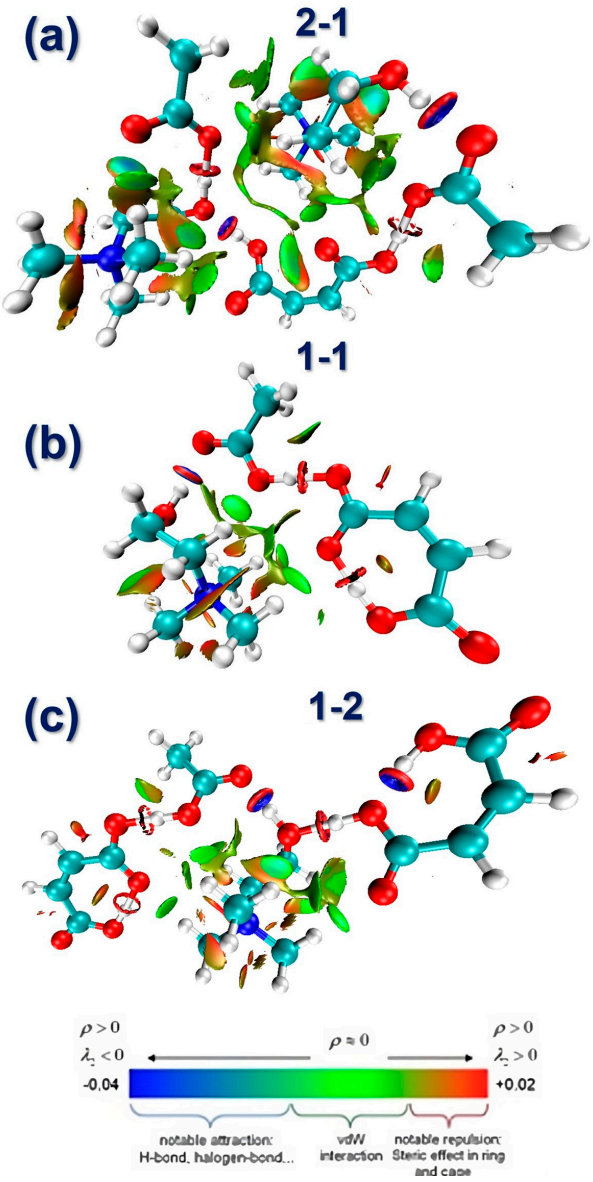

Figure 3. NCI surface computed for 2-1 (**a**), 1-1 (**b**) and 1-2 (**c**) compositions. All calculations are referred to the most stable configuration of each composition. (Isovalue = 0.75).

3.2. Infrared Spectroscopy Results

Figure 4 shows the experimental FIR absorbance spectra (panel a) measured at 300K for the three considered concentrations, and the theoretically computed spectra (panel b, c and d for ChAc-MA 2-1,ChAc-MA 1-1 and ChAc-MA 1-2, respectively).

The experimental spectra of the three samples are qualitatively very similar, as they all show an absorption band around 100 cm^{-1}, which is particularly pronounced in the 1-1 and 2-1 compositions. The high frequency side of this band presents a shoulder around 180 cm^{-1} which is detectable as a well distinguishable band in the ChAc-MA 1-2 mixture. At higher frequencies, all the three spectra show a wide band between 300 and 400 cm^{-1} whose maximum shifts to lower frequencies with increasing acid content, and a couple of minor bands between 400 and 500 cm^{-1}, which become closer at higher acid contents and overlap in the ChAc-MA 1-2 mixture.

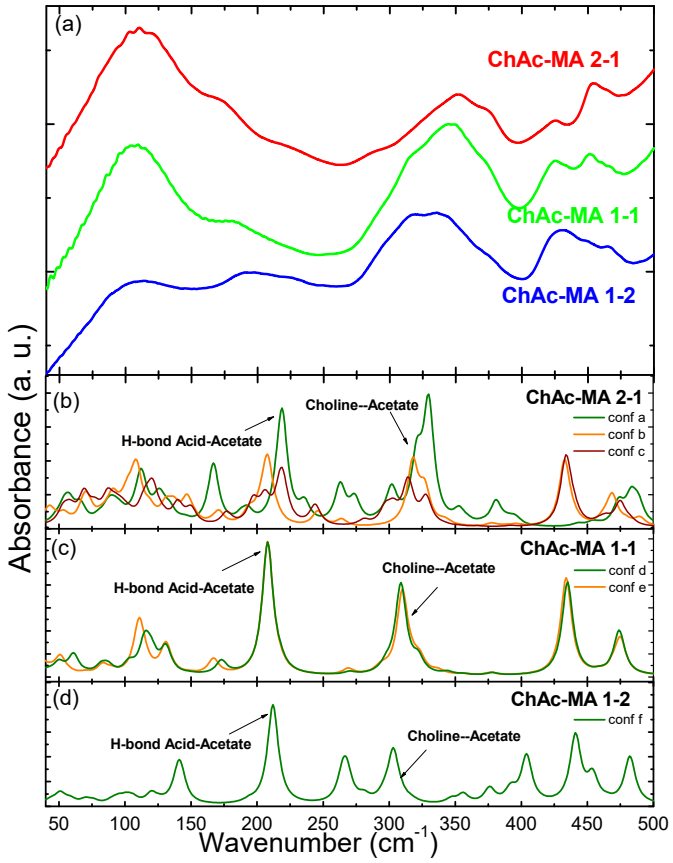

Figure 4. Room temperature experimental (**a**) and computational (**b**–**d**) FIR absorbance of ChAc-MA mixtures.

The band around 100 cm^{-1} appeared challenging to be assigned: the computational models of the three mixtures suggest that it is generated by the superposition of several contributions related to skeletal movements of the components and intermolecular interactions. In particular, numerous signals are noticeable in the computational spectra of the 2-1 composition around this frequency. This arises from the great number of degrees of freedom within the molecular cluster, resulting in a higher number of possible vibrational modes. As described by Fumino and coworkers for protic ionic liquids [24], the band around 100 cm^{-1} can be interpreted as originating from dispersion forces between the components of mixtures. This interpretation is supported by the calculation of Non-Covalent Interactions reported in Figure 3: the extended green region observable in NCI surfaces corresponds to van der Waals interactions, or more broadly, to regions characterized by dispersion force interactions. Although a strictly quantitative interpretation of intermolecular interactions by means of the NCI method is not feasible, we noted that in the 2-1 composition, the green-colored zones are broader and their extension tends to decrease as the amount of choline acetate in the mixtures decreases. Indeed, in the experimental spectra, we observed that the intensity of the dispersion forces band seems to follow the same described trend, since it is the most intense band of the measured frequency range in the 2-1 composition, while its intensity is comparable to that of the other bands in the 1-1 composition and becomes broader and less intense than the other absorptions in the 1-2 mixture. The computational investigation predicted the presence of a robust hydrogen bonding network between the components comprising the mixtures. Since infrared spectroscopy is a proven method to detect hydrogen bonding in liquid systems [24,25,52] from an experimental perspective, we expected to observe well-defined signals associated with hydrogen bond stretching in the region below 200cm^{-1}. Instead, the experimental FIR spectra exhibited only broad bands between 185 and 175 cm^{-1}. The broad shape of

these bands, notably pronounced in the 1-2 composition, presented a notable challenge in precisely determining the peak maximum. The computational spectra revealed a prominent signal slightly below 200cm^{-1}: our DFT calculations suggested they can be attributed to the stretching of hydrogen bonds between maleic acid and acetate. These frequencies are compatible with the occurrence of strong hydrogen bonding as confirmed by the comparison with similar results in protic and aprotic ionic liquids [24,25,52]. Moreover, as the concentration of the acid in the mixtures increases, the bands of the H-bond stretching appear blue-shifted. This phenomenon can be rationalized as an increase in the strength of the hydrogen bonding at high acid concentrations. In other words, we can hypothesize that an increased concentration of acid facilitates the donation of more H-bonds, consequently fostering the establishment of a more intense network of intermolecular contacts. The characterization of H-bond bending motions presented a greater complexity: our calculations suggested the existence of these vibrations at low wavenumbers overlapping with the broad band at 100 cm^{-1}.

It is worth noticing that the shape of the bands below 200cm^{-1} did not change at a lower temperature, as shown in Figure 5, which reports the thermal evolution of the FIR spectra acquired on heating between 120 and 320 K. Except for the band at 350 cm^{-1} of the 1-2 sample, the experimental spectra do not show significant differences in the shape and position of the bands between high and low temperatures. This is consistent with the formation of a glassy phase, since, when first-order phase transition such as solidification or melting occurs, the shape and position of the peaks change significantly [26,27]

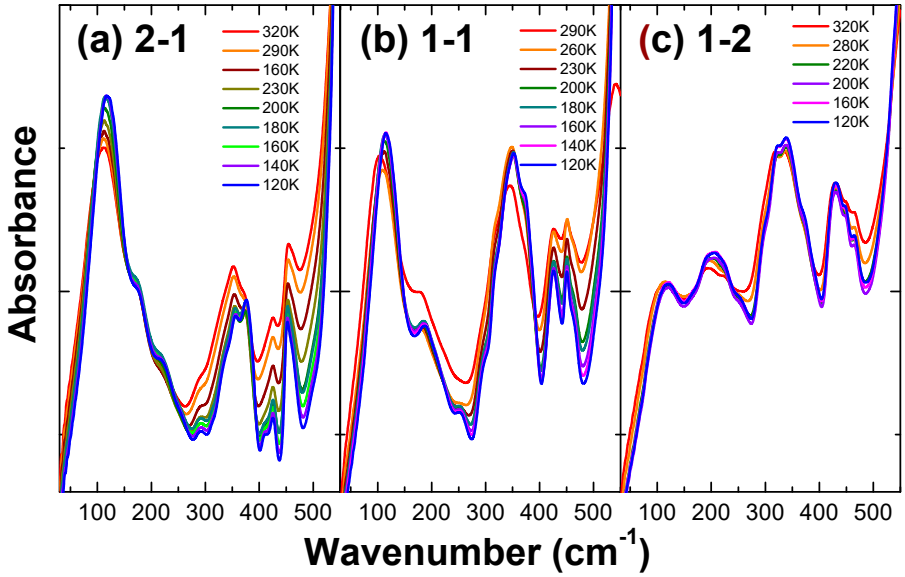

Figure 5. Temperature dependence of the infrared absorption spectra of 2-1 (**a**), 1-1 (**b**) and 1-2 (**c**) composition measured on heating.

Indeed, the studied mixtures do not crystallize on cooling but rather undergo a glass transition, as witnessed by the Differential Scanning Calorimetry (DSC) curves reported in the SI (Figure S1). Therefore, in the present case, the shape of the bands due to intermolecular interactions does not change appreciably. On the contrary, in ionic liquids, the presence of hydrogen bonding was more evident from the spectra collected at low temperatures and in the solid state [25,52], where the high directionality of the H-bonding was easily detected.

Figure 5a also shows that the shape of the asymmetric peak centered around 350 cm^{-1} varies with temperature: at low temperatures, it appears as a structured peak in which distinct contributions can be distinguished. The relative weights of these bands change as the temperatures increases, and when it is close to RT, the different contributions overlap and become almost indistinguishable. This band is detected for all the compositions (Figure 5),

but its shape is different in the different composition; in the 1-1 and 1-2 composition, one cannot appreciate the presence of two well-separated bands. Its modification with the temperature is clearly evident only in the 2-1 mixture (Figure 5a), while it is almost absent in the 1-1 (Figure 5b) and 1-2 (Figure 5c) mixtures. Previous DSC results (Figure S1) clearly exclude that these changes are due to phase transitions. A reasonable explanation for the change in the shape of the bands of the 2-1 composition as a function of temperature could be made by considering that such signals originated from the thermal evolution of the population of different geometric configurations. Indeed, it is widely recognized that the relative weight of each configuration in liquid phase depends on the Boltzmann distribution. As the temperature changes, the population of each level changes until a solid or glassy phase forms. In this phase, the configuration changes no longer follow the Boltzmann distribution and instead become frozen. Our DFT modeling suggested that the band around 350 cm^{-1} arises from the superimposing contributions coming from different conformers. Indeed, although the univocal assignments of bands based on theoretical spectra were particularly challenging, the computational spectra clearly indicated that in the considered frequency range each of the configurations obtained from DFT generate a band (see Figure 4), mainly due to the vibrations of the choline acetate,although this also involves maleic acid.

In particular, for the ChAc-MA 2-1 mixture, Figure 4b shows that all the three conformers (Figure 2a–c) present different peaks in correspondence to the broad band around 350cm^{-1}. Conversely, the two configurations obtained for the ChAc-MA 1-1 mixture (Figure 2d,e) are characterized by a very similar spectrum (Figure 4c) and one cannot distinguish different contributions around 350 cm^{-1}. Actually, the shape of the peak around 350 cm^{-1} in the spectrum of the ChAc-MA 1-1 mixture does not appreciably change with temperature and, indeed, this is highly expected since the two configurations are almost coincident and separated by an extremely low energy difference.

To further investigate if the changes in temperature in the band intensity are given by the modification of the configurations distributions, the band profile was analyzed with the same model already used for other systems [53,54]. Indeed, in a liquid, the ratio (r) between two specific configuration concentrations is proportional to the ratio of the intensities of their bands and can be defined as reported in Equation (3):

$$r = \frac{I_1}{I_2} \tag{3}$$

where I_1 and I_2 are the integrated IR intensity of the bands corresponding to the different configurations. The thermodynamic equilibrium constant K between configurations is proportional to r and depends on ΔG^0, as reported in Equation (4):

$$-RTln(r) = \Delta G^0 = \Delta H^0 - T\Delta S^0 \tag{4}$$

where R is the gas constant, T is the temperature and DH^0 and DS^0 are the enthalpy and entropy difference in the configurations; it can be rearranged as

$$ln(r) = -\frac{1}{T}\frac{\Delta H^0}{R} + \frac{\Delta S^0}{R} + c \tag{5}$$

where c is a constant. Plotting $ln(r)$ as a function of $1/T$ allows to verify the van't Hoff dependence of the concentration from the temperature evolution. The slope of the linear regression of $ln(r)$ provides the values of energy separation between the two configurations.

In order to use this model to verify our hypothesis, the experimental band observed in the ChAc-MA 2-1 mixture was deconvoluted after a baseline correction, using three Gaussian functions centered at about 340 cm^{-1}, 360 cm^{-1} and 380 cm^{-1}, respectively: indeed, the 2-1 composition presented three different possible geometric configurations within the energy range that was considered by us. Although the structures slightly differ from a geometric point, vibrational frequency calculations provided clues suggesting that

each of them are capable of generating a different band in the spectral region between 300 and 400 cm^{-1}. Figure 6 reports the van't Hoff plot obtained from the calculated values of the $ln(r)$ related to compositions 2-1.

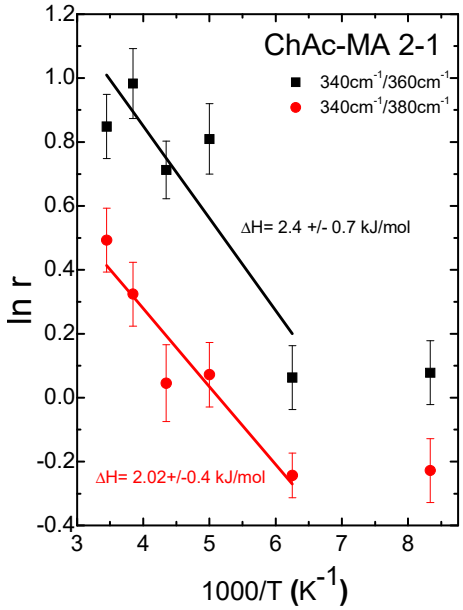

Figure 6. van't Hoff plot of the ratio of the intensities of bands generated by the conformations of ChAc-MA 2-1.

Two regression fits were performed using the ratio between the bands at 360 cm^{-1} and 340 cm^{-1} (black square, Figure 6) and 380 cm^{-1} and 340 cm^{-1} (red circle, Figure 6). In both cases, we observed a good linearity between $ln(r)$ and $1/T$, with the best fit obtained for 380/340 cm^{-1}. In particular, Figure 6 shows a linear relationship between $ln(r)$ and $1/T$ from room temperature to approximately 185K, while a notable deviation from linearity is observed below this value. This kind of dependence was typically observed in ionic liquids undergoing a glass transition: the liquid phase is characterized by a linear dependence of ln(r) while a substantial deviation from linearity is observed in the low temperature glassy phase. Indeed, the evolution of conformers according to a Boltzmann distribution is only applicable within the liquid phase: upon the formation of solid or vitreous phases, geometric conformations become fixed into a single geometry. It is worth noting that linear dependence is not observed below 185K, which is very close to the glass transition temperature reported by DSC (around 190K in Figure S1).

The slope of the linear regression of $ln(r)$ vs. $1/T$ provides an evaluation of the energy separation between the energy level of geometrical configurations in the liquid, ΔH^0.

Both regressions produce similar values of ΔH^0, although the standard deviation on the fit reported in Figure 6 suggests that the best linear regression occurs for the ratio calculated between the bands at 380 cm^{-1} and 340 cm^{-1}. The obtained values are comparable to the energy differences provided by DFT. Indeed, considering that the two configurations are very close in energy (0.8 kJ/mol), it is reasonable that the two considered couples provided similar energy differences. Moreover, the calculated spectrum of the three configurations (Figure 3b) presents several peaks in the analyzed frequency range, making the exact attribution of each one of the deconvoluted lines to a specific configurationdifficult. However, the obtained dependence is in agreement with the calculation results. It is worth noting that in the composition 1-2, the band around 350 cm^{-1} did not exhibit significant variations with changing temperatures, as the relative weight of the possible components of the band remained practically unchanged. This result can be explained considering that no population redistribution can be possible, as confirmed by the DFT calculations, which indicated the presence of a single possible conformation (configuration

f in Figure 2) and provides further confirmation of the computational results. Indeed, in the previous paragraph, we noted a decrease in the number of energetically accessible molecular conformations as the quantity of acid molecules within the mixtures increased. We explained this evidence by considering that as the acid concentration increased, there was a corresponding rise in the number of hydrogen bond donor groups. These additional hydrogen bonds could result in more rigid structures and geometries due to enhanced cross-linking. The spectroscopic results described so far seem to support our interpretation.

4. Conclusions

DFT calculations allowed the description of the low energy configurations of the mixed ChAc-MA system. We found that the available number of these configurations decreases with the increase in the acid content. Moreover, the formation of intramolecular hydrogen bonding was observed within the maleic acid in all configurations, except the most stable one of the mixtures with the lowest acid content. This intramolecular hydrogen bonding seems to favor the establishment of a proton transfer mechanism, thus suggesting a new role in these kinds of mixtures for the already well-studied subject of hydrogen bonding.

The increased stability observed at low acid content for the configuration lacking the acid intramolecular hydrogen bonding may arise from the open structure of the acid, facilitating more efficient cross-linking and the structural stabilization of the whole system.

NCI analysis indicates that, besides the hydrogen bonds which contribute significantly to the stabilization effect in these mixtures, the van der Waals interactions also contribute to the determination of the equilibrium geometries. The role of these interactions has usually been less considered by the previous literature.

Far-infrared measurements provided information about the temperature evolution of the possible configurations, further confirming calculation results.

The combined use of calculations and far-infrared experiments appears effective in the study of the intermolecular interactions in mixed systems and could be used in a wide range of promising solvents.

Supplementary Materials: The following supporting information can be downloaded at https://www.mdpi.com/article/10.3390/app142311402/s1: Figure S1: DSC curves on heating (5 K/min) for the studied mixtures. Table S1: Distances and angles of the characteristic bonds of the low energy configurations obtained for the three mixtures. Table S2: Absolute energy in kJ/mol obtained at B3LYP/6-31G** level of theory for the low energy configurations of ChAc-MA 2-1, ChAc-MA 1-1 and ChAc-MA 1-2.

Author Contributions: Conceptualization, O.P. and S.D.M.; methodology, O.P. and A.P.; validation, O.P., S.D.M. and F.T.; formal analysis, O.P. and S.D.M.; investigation, S.D.M. and F.T.; resources, A.P.; data curation, O.P. and S.D.M. writing—original draft preparation, S.D.M. and O.P.; writing—review and editing, all authors; supervision, O.P. and A.P.; funding acquisition, A.P. All authors have read and agreed to the published version of the manuscript.

Funding: This research received no external funding.

Institutional Review Board Statement: Not applicable.

Informed Consent Statement: Not applicable.

Data Availability Statement: Data are contained within the article or Supplementary Materials.

Acknowledgments: The authors acknowledge SOLEIL for the provision of synchrotron radiation facilities and they would like to thank Pascale Roy and Jean-Blaise Brubach for assistance in using beamline AILES during beamtime 20231279 and 20230398.

Conflicts of Interest: The authors declare no conflicts of interest.

References

1. Dai, Y.; Van Spronsen, J.; Witkamp, G.J.; Verpoorte, R.; Choi, Y.H. Ionic Liquids and Deep Eutectic Solvents in Natural Products Research: Mixtures of Solids as Extraction Solvents. *J. Nat. Prod.* **2013**, *76*, 2162–2173. [CrossRef] [PubMed]

2. Li, K.; Zong, K.; Wang, X.; Cui, G.; Deng, D. Ionic Liquids and Deep Eutectic Solvents for NH3 Absorption and Separation: A Review. *New J. Chem.* **2023**, *47*, 21426–21445. [CrossRef]
3. Chen, Y.; Mu, T. Revisiting Greenness of Ionic Liquids and Deep Eutectic Solvents. *Green Chem. Eng.* **2021**, *2*, 174–186. [CrossRef]
4. Sun, J.; Sato, Y.; Sakai, Y.; Kansha, Y. A Review of Ionic Liquids and Deep Eutectic Solvents Design for CO_2 Capture with Machine Learning. *J. Clean. Prod.* **2023**, *414*, 137695. [CrossRef]
5. Omar, K.A.; Sadeghi, R. Database of Deep Eutectic Solvents and Their Physical Properties: A Review. *J. Mol. Liq.* **2023**, *384*, 121899. [CrossRef]
6. Omar, K.A.; Sadeghi, R. Physicochemical Properties of Deep Eutectic Solvents: A Review. *J. Mol. Liq.* **2022**, *360*, 119524. [CrossRef]
7. Fumino, K.; Peppel, T.; Geppert-Rybczyńska, M.; Zaitsau, D.H.; Lehmann, J.K.; Verevkin, S.P.; Köckerling, M.; Ludwig, R. The Influence of Hydrogen Bonding on the Physical Properties of Ionic Liquids. *Phys. Chem. Chem. Phys.* **2011**, *13*, 14064–14075. [CrossRef]
8. El Achkar, T.; Greige-Gerges, H.; Fourmentin, S. Basics and Properties of Deep Eutectic Solvents: A Review. *Environ. Chem. Lett.* **2021**, *19*, 3397–3408. [CrossRef]
9. Zhang, S.; Sun, N.; He, X.; Lu, X.; Zhang, X. Physical Properties of Ionic Liquids: Database and Evaluation. *J. Phys. Chem. Ref. Data* **2006**, *35*, 1475–1517. [CrossRef]
10. Deetlefs, M.; Seddon, K.R.; Shara, M. Predicting Physical Properties of Ionic Liquids. *Phys. Chem. Chem. Phys.* **2006**, *8*, 642–649. [CrossRef]
11. Domańska, U. Solubilities and Thermophysical Properties of Ionic Liquids. *Pure Appl. Chem.* **2005**, *77*, 543–557. [CrossRef]
12. Smith, E.L.; Abbott, A.P.; Ryder, K.S. Deep Eutectic Solvents (DESs) and Their Applications. *Chem. Rev.* **2014**, *114*, 11060–11082. [CrossRef] [PubMed]
13. Afonso, J.; Mezzetta, A.; Marrucho, I.M.; Guazzelli, L. History Repeats Itself Again: Will the Mistakes of the Past for ILs Be Repeated for DESs? From Being Considered Ionic Liquids to Becoming Their Alternative: The Unbalanced Turn of Deep Eutectic Solvents. *Green Chem.* **2022**, *25*, 59–105. [CrossRef]
14. Xu, P.; Zheng, G.W.; Zong, M.H.; Li, N.; Lou, W.Y. Recent Progress on Deep Eutectic Solvents in Biocatalysis. *Bioresour. Bioprocess.* **2017**, *4*, 34. [CrossRef]
15. Bashir, I.; Dar, A.H.; Dash, K.K.; Pandey, V.K.; Fayaz, U.; Shams, R.; Srivastava, S.; Singh, R. Deep Eutectic Solvents for Extraction of Functional Components from Plant-Based Products: A Promising Approach. *Sustain. Chem. Pharm.* **2023**, *33*, 101102. [CrossRef]
16. García, A.; Rodríguez-Juan, E.; Rodríguez-Gutiérrez, G.; Rios, J.J.; Fernández-Bolaños, J. Extraction of Phenolic Compounds from Virgin Olive Oil by Deep Eutectic Solvents (DESs). *Food Chem.* **2016**, *197*, 554–561. [CrossRef]
17. Toledo Hijo, A.A.C.; Alves, C.; Farias, F.O.; Peixoto, V.S.; Meirelles, A.J.A.; Santos, G.H.F.; Maximo, G.J. Ionic Liquids and Deep Eutectic Solvents as Sustainable Alternatives for Efficient Extraction of Phenolic Compounds from Mate Leaves. *Food Res. Int.* **2022**, *157*, 111194. [CrossRef]
18. Sakhno, T.V.; Barashkov, N.N.; Irgibaeva, I.S.; Mendigaliyeva, S.; Bostan, D.S. Ionic Liquids and Deep Eutectic Solvents and Their Use for Dissolving Animal Hair. *Adv. Chem. Eng. Sci.* **2020**, *10*, 40–51. [CrossRef]
19. Quintana, A.A.; Sztapka, A.M.; Santos Ebinuma, V.d.C.; Agatemor, C. Enabling Sustainable Chemistry with Ionic Liquids and Deep Eutectic Solvents: A Fad or the Future? *Angew. Chem. Int. Ed.* **2022**, *61*, e202205609. [CrossRef]
20. Hammond, O.S.; Mudring, A.V. Ionic Liquids and Deep Eutectics as a Transformative Platform for the Synthesis of Nanomaterials. *Chem. Commun.* **2022**, *58*, 3865–3892. [CrossRef]
21. Swebocki, T.; Barras, A.; Abderrahmani, A.; Haddadi, K.; Boukherroub, R. Deep Eutectic Solvents Comprising Organic Acids and Their Application in (Bio)Medicine. *Int. J. Mol. Sci.* **2023**, *24*, 8492. [CrossRef] [PubMed]
22. Di Muzio, S.; Palumbo, O.; Trequattrini, F.; Paolone, A. Binary Mixtures of Choline Acetate and Tetrabutylammonium Acetate with Natural Organic Acids by Vibrational Spectroscopy and Molecular Dynamics Simulations. *J. Phys. Chem. B* **2024**, *128*, 857–870. [CrossRef] [PubMed]
23. Ferreira, E.S.C.; Voroshylova, I.V.; Figueiredo, N.M.; Cordeiro, M.N.D.S. Molecular Dynamic Study of Alcohol-Based Deep Eutectic Solvents. *J. Chem. Phys.* **2021**, *155*, 064506. [CrossRef] [PubMed]
24. Fumino, K.; Fossog, V.; Stange, P.; Paschek, D.; Hempelmann, R.; Ludwig, R. Controlling the Subtle Energy Balance in Protic Ionic Liquids: Dispersion Forces Compete with Hydrogen Bonds. *Angew. Chem. Int. Ed.* **2015**, *54*, 2792–2795. [CrossRef]
25. Palumbo, O.; Cimini, A.; Trequattrini, F.; Brubach, J.B.; Roy, P.; Paolone, A. The Infrared Spectra of Protic Ionic Liquids: Performances of Different Computational Models to Predict Hydrogen Bonds and Conformer Evolution. *Phys. Chem. Chem. Phys.* **2020**, *22*, 7497–7506. [CrossRef]
26. Palumbo, O.; Sarra, A.; Brubach, J.B.; Trequattrini, F.; Cimini, A.; Brutti, S.; Appetecchi, G.B.; Simonetti, E.; Maresca, G.; Fantini, S.; et al. So Similar, yet so Different: The Case of the Ionic Liquids N-Trimethyl-N (2-Methoxyethyl)Ammonium Bis (Trifluoromethanesulfonyl)Imide and N,N-Diethyl-N-Methyl-N(2-Methoxyethyl)Ammonium Bis(Trifluoromethanesulfonyl)Imide. *Front. Phys.* **2022**, *10*, 851279. [CrossRef]
27. Palumbo, O.; Trequattrini, F.; Cimini, A.; Tsurumaki, A.; Navarra, M.A.; Paolone, A. Inter- and Intramolecular Interactions in Ether-Functionalized Ionic Liquids. *J. Phys. Chem. B* **2021**, *125*, 2380–2388. [CrossRef]
28. Ozaki, Y. Infrared Spectroscopy—Mid-Infrared, Near-Infrared, and Far-Infrared/Terahertz Spectroscopy. *Anal. Sci.* **2021**, *37*, 1193–1212. [CrossRef]

29. Bakker, D.J.; Dey, A.; Tabor, D.P.; Ong, Q.; Mahé, J.; Gaigeot, M.P.; Sibert, E.L.; Rijs, A.M. Fingerprints of Inter- and Intramolecular Hydrogen Bonding in Saligenin-Water Clusters Revealed by Mid- and Far-Infrared Spectroscopy. *Phys. Chem. Chem. Phys.* **2017**, *19*, 20343–20356. [CrossRef]
30. El Khoury, Y.; Hellwig, P. Far Infrared Spectroscopy of Hydrogen Bonding Collective Motions in Complex Molecular Systems. *Chem. Commun.* **2017**, *53*, 8389–8399. [CrossRef]
31. Brubach, J.B.; Mermet, A.; Filabozzi, A.; Gerschel, A.; Lairez, D.; Krafft, M.P.; Roy, P. Dependence of Water Dynamics upon Confinement Size. *J. Phys. Chem. B* **2001**, *105*, 430–435. [CrossRef]
32. D'Angelo, G.; Conti Nibali, V.; Crupi, C.; Rifici, S.; Wanderlingh, U.; Paciaroni, A.; Sacchetti, F.; Branca, C. Probing Intermolecular Interactions in Phospholipid Bilayers by Far-Infrared Spectroscopy. *J. Phys. Chem. B* **2017**, *121*, 1204–1210. [CrossRef] [PubMed]
33. Dominguez-Vidal, A.; Kaun, N.; Ayora-Cañada, M.J.; Lendl, B. Probing Intermolecular Interactions in Water/Ionic Liquid Mixtures by Far-Infrared Spectroscopy. *J. Phys. Chem. B* **2007**, *111*, 4446–4452. [CrossRef]
34. Bakker, D.J.; Peters, A.; Yatsyna, V.; Zhaunerchyk, V.; Rijs, A.M. Far-Infrared Signatures of Hydrogen Bonding in Phenol Derivatives. *J. Phys. Chem. Lett.* **2016**, *7*, 1238–1243. [CrossRef] [PubMed]
35. Brubach, J.B.; Mermet, A.; Filabozzi, A.; Gerschel, A.; Roy, P. Signatures of the Hydrogen Bonding in the Infrared Bands of Water. *J. Chem. Phys.* **2005**, *122*, 184509. [CrossRef] [PubMed]
36. Walther, M.; Fischer, B.M.; Jepsen, P.U. Noncovalent Intermolecular Forces in Polycrystalline and Amorphous Saccharides in the Far Infrared. *Chem. Phys.* **2003**, *288*, 261–268. [CrossRef]
37. Marekha, B.A.; Kalugin, O.N.; Idrissi, A. Non-Covalent Interactions in Ionic Liquid Ion Pairs and Ion Pair Dimers: A Quantum Chemical Calculation Analysis. *Phys. Chem. Chem. Phys.* **2015**, *17*, 16846–16857. [CrossRef]
38. Contreras-García, J.; Boto, R.A.; Izquierdo-Ruiz, F.; Reva, I.; Woller, T.; Alonso, M. A Benchmark for the Non-Covalent Interaction (NCI) Index Or. . . Is It Really All in the Geometry? *Theor. Chem.Acc.* **2016**, *135*, 242. [CrossRef]
39. Alkorta, I.; Elguero, J.; Frontera, A. Not Only Hydrogen Bonds: Other Noncovalent Interactions. *Crystals* **2020**, *10*, 180. [CrossRef]
40. Ohno, K.; Oki, T.; Yamakado, H. Quantum Chemical Exploration of Intermolecular Reactions of Acetylene. *J. Comput. Chem.* **2020**, *41*, 687–697. [CrossRef]
41. Otero-De-La-Roza, A.; Johnson, E.R.; Contreras-García, J. Revealing Non-Covalent Interactions in Solids: NCI Plots Revisited. *Phys. Chem. Chem. Phys.* **2012**, *14*, 12165–12172. [CrossRef] [PubMed]
42. Wakai, C.; Oleinikova, A.; Ott, M.; Weinga, H. How Polar Are Ionic Liquids? Determination of the Static Dielectric Constant of an Imidazolium-Based Ionic Liquid by Microwave Dielectric Spectroscopy. *J. Phys. Chem. B* **2005**, *109*, 17028–17030. [CrossRef] [PubMed]
43. Singh, T.; Kumar, A. Static Dielectric Constant of Room Temperature Ionic Liquids: Internal Pressure and Cohesive Energy Density Approach. *J. Phys. Chem. B* **2008**, *112*, 12968–12972. [CrossRef] [PubMed]
44. Palumbo, O.; Vitucci, F.M.; Trequattrini, F.; Paolone, A. A Study of the Conformers of the N,N-Diethyl-N-Methyl-N-Propylammonium Ion by Means of Infrared Spectroscopy and DFT Calculations. *Vib. Spectrosc.* **2015**, *80*, 11–16. [CrossRef]
45. Shao, Y.; Molnar, L.F.; Jung, Y.; Kussmann, J.; Ochsenfeld, C.; Brown, S.T.; Gilbert, A.T.B.; Slipchenko, L.V.; Levchenko, S.V.; O'Neill, D.P.; et al. Advances in Methods and Algorithms in a Modern Quantum Chemistry Program Package. *Phys. Chem. Chem. Phys.* **2006**, *8*, 3172–3191. [CrossRef]
46. Lu, T.; Chen, F. Multiwfn: A Multifunctional Wavefunction Analyzer. *J. Comput. Chem.* **2012**, *33*, 580–592. [CrossRef]
47. Humphrey, W.; Dalke, A.; Schulten, K. VMD: Visual Molecular Dynamics. *J. Mol. Graph.* **1996**, *14*, 33–38. [CrossRef]
48. Jeffrey, G.A. *An Introduction to Hydrogen Bonding*; Oxford University Press: New York, NY, USA, 1997.
49. Arunan, E.; Desiraju, G.R.; Klein, R.A.; Sadlej, J.; Scheiner, S.; Alkorta, I.; Clary, D.C.; Crabtree, R.H.; Dannenber, J.J.; Hobza, P.; et al. Definition of the Hydrogen Bond (IUPAC Recommendations 2011). *Pure Appl. Chem.* **2011**, *83*, 1637–1641. [CrossRef]
50. Di Muzio, S.; Ramondo, F.; Gontrani, L.; Ferella, F.; Nardone, M.; Benassi, P. Choline Hydrogen Dicarboxylate Ionic Liquids by X-Ray Scattering, Vibrational Spectroscopy and Molecular Dynamics: H-Fumarate and H-Maleate and Their Conformations. *Molecules* **2020**, *25*, 4990. [CrossRef]
51. Smith, M.B. *Organic Chemistry: An Acid–Base Approach*; CRC Press: Boca Raton, FL, USA, 2023; ISBN 9781000601312.
52. Palumbo, O.; Cimini, A.; Trequattrini, F.; Brubach, J.B.; Roy, P.; Paolone, A. Evidence of the Ch···O Hydrogenbonding in Imidazolium-based Ionic Liquids from Far-infrared Spectroscopy Measurements and Dft Calculations. *Int. J. Mol. Sci.* **2021**, *22*, 6155. [CrossRef]
53. Capitani, F.; Gatto, S.; Postorino, P.; Palumbo, O.; Trequattrini, F.; Deutsch, M.; Brubach, J.B.; Roy, P.; Paolone, A. The Complex Dance of the Two Conformers of Bis(Trifluoromethanesulfonyl)Imide as a Function of Pressure and Temperature. *J. Phys. Chem. B* **2016**, *120*, 1312–1318. [CrossRef]
54. Palumbo, O.; Trequattrini, F.; Vitucci, F.M.; Navarra, M.A.; Panero, S.; Paolone, A. An Infrared Spectroscopy Study of the Conformational Evolution of the Bis(Trifluoromethanesulfonyl)Imide Ion in the Liquid and in the Glass State. *Adv. Condens. Matter Phys.* **2015**, *2015*, 176067. [CrossRef]